Stabilization of the $n = 3$ Ruddlesden−Popper Phases: $Sr_4Mn_{3-x}Fe_xO_{10-\delta}$ and $Sr_{4-y}Ca_yMn_3O_{10-\delta}$

Rongji Chen and Martha Greenblatt*

Department of Chemistry, Rutgers, the State University of New Jersey, Piscataway, New Jersey 08854-8087

Leonid A. Bendersky

Metallurgy Division, NIST, 100 Bureau Drive, Stop 8554, Gaithersburg, Maryland 20899-8554

Received April 3, 2001. Revised Manuscript Received July 24, 2001

$Sr_4Mn_3O_{10}$, which crystallizes in space group *Cmca*, is not a Ruddlesden−Popper (RP) phase. The partial substitution of either Mn by Fe or Sr by Ca leads to a stable $n = 3$ RP phase with tetragonal symmetry (*I*4/*mmm*). The minimum amount of Fe or Ca needed to obtain a stable RP phase is $x = 0.40$ for $Sr_4Mn_{3-x}Fe_xO_{10-\delta}$ and $y = 2.85$ for $Sr_{4-y}Ca_yMn_3O_{10-\delta}$. High-resolution transmission electron microscopy and selected area electron diffraction electron microscopy indicate that about 50% of the grains have well-ordered $n = 3$ structure for both series of RP phases, while the rest of the grains show significant intergrowth between the $n = 2$ and $n = 3$ structures. $Sr_4Mn_{2.6}Fe_{0.4}O_{10-\delta}$ and $Sr_{1.15}Ca_{2.85}Mn_3O_{10-\delta}$ are semiconductors and exhibit spin-glass like transitions at low temperature.

Introduction

The general formula $(AO)(ABO_3)_n$ ($n = 1, 2, 3, \ldots \infty$) represents the family of compounds known as Ruddlesden−Popper (RP) phases. The structure consists of perovskite blocks, *n* octahedra thick, separated by rock salt AO layers. Following the discovery of colossal magnetoresistance (CMR) in perovskites of the form $Ln_{1-x}A_xMnO_3$, the layered members of the RP series have been extensively studied. Alteration of rock-salt AO layers between perovskite-like layers results in a two-dimensional (2D) character and a reduction from six to five of the number of nearest-neighbor manganese atoms around sites at the edge of the $(ABO_3)_n$ slabs in the layered RP phases ($n < \infty$). In the quasi-low-dimensional RP systems, due to anisotropic exchange interactions, electronic correlations are enhanced and unique magnetotransport behavior is expected.

The RP phases $(AO)(AMnO_3)_n$, with A = Ca, can be obtained relatively easily by conventional synthetic methods. In case of A = Sr, it is much more difficult to synthesize a RP phase. α-$SrMnO_{3-\delta}$ is a hexagonal perovskite formed by chains of face-sharing octahedra.[1−5] Sr_2MnO_4 exists in two forms: a low-temperature α-Sr_2MnO_4 (similar to α-$SrMnO_{3-\delta}$) and a high-temperature *β*-Sr_2MnO_4 (K_2NiF_4-type structure, RP phase).[6,7] The α→*β* transformation takes place at ∼1600 °C. *β*-Sr_2MnO_4 was obtained by quenching from high temperature to room temperature;[6,7] when *β*-Sr_2MnO_4 is annealed for at least 8 h at 1200 °C, it transforms to α-Sr_2MnO_4.[7] The RP phase $Sr_3Mn_2O_7$ was first reported by Mizutani et al.;[8] it is metastable below 1600 °C and must be quenched from 1600 °C into dry ice to prevent its decomposition to α-Sr_2MnO_4 and $Sr_4Mn_3O_{10}$.[9]

Attempts to synthesize the $n = 3$ member $Sr_4Mn_3O_{10}$ in air led to the formation of an oxycarbonate, $Sr_5Mn_4CO_3O_{10}$.[10] The layered manganate $Sr_4Mn_3O_{10}$ in space group *Cmca* was first grown from melts in platinum crucibles with $SrCl_2/SrF_2$ as solvent by Fabry et al.[11] It is orthorhombic (*Cmca*) with triple groups of face-shared MnO_6 octahedra linked up by common corners of terminal octahedra into a two-dimensional framework structure perpendicular to the [010] direction. The incorporation of a trace amount of platinum (from the container) or some other transition metals appeared to play an essential role in the formation of the orthorhombic $Sr_4Mn_3O_{10}$ phase. Recently, Floros et al.[12] reported the formation of pure $Sr_4Mn_3O_{10}$ and $Sr_{4-x}Ba_xMn_3O_{10}$ ($0 \le x \le 2.5$) orthorhombic-layered phases without platinum doping under carefully controlled conditions.

Recently we have reported on the synthesis and properties of RP $Sr_4Mn_{3-x}Fe_xO_{10-\delta}$ ($x = 1, 1.5, 2$) and

* Corresponding author. E-mail: greenblatt@rutchem.rutgers.edu.

(1) Syono, Y.; Akimoto, S. *J. Phys. Soc. Jpn.* **1969**, *26*, 993.
(2) Negas, T.; Roth, R. S. *J. Solid State Chem.* **1970**, *1*, 409.
(3) Negas, T.; Roth, *J. Solid State Chem.* **1971**, *3*, 323.
(4) Kuroda, K.; Ishizawa, N.; Mizutani, N.; Kato, M. *J. Solid State Chem.* **1981**, *38*, 297.
(5) Battle, P. D.; Gibb, T. C.; Jones, C. W. *J. Solid State Chem.* **1988**, *74*, 60.
(6) Baltz, D.; Plieth, K. *Z. Electrochem.* **1955**, *59*, 545.
(7) Bouloux, J.-C.; Soubeyroux, J.-L.; Flem, G. L.; Hagenmuller, P. *J. Solid State Chem.* **1981**, *38*, 34.
(8) Mizutani, N.; Kitazawa, A.; Nobuyuki O.; Kato, M. *J. Chem. Soc. (Jpn.) In. Ed.* **1970**, *73*, 1097.
(9) Mitchell, J. F.; Millburn, J. E.; Medarde, M.; Short S.; Jorgensen, J. D. *J. Solid State Chem.* **1998**, *141*, 599.
(10) Caignaert, V.; Domenges, B.; Raveau, B. *J. Solid State Chem.* **1995**, *120*, 279.
(11) Fábry, J.; Hybler, J.; Jirák, Z.; Jurek, K.; Malý, K.; Nevriva, M.; Petrícek, V. *J. Solid State Chem.* **1988**, *73*, 520.
(12) Floros, N.; Hervieu, M.; Tendeloo, G. V.; Michel, C.; Maignan, A.; Raveau, B. *Solid State Sci.* **2000**, *2*, 1.

10.1021/cm0102842 CCC: $20.00
Published on Web 09/19/2001

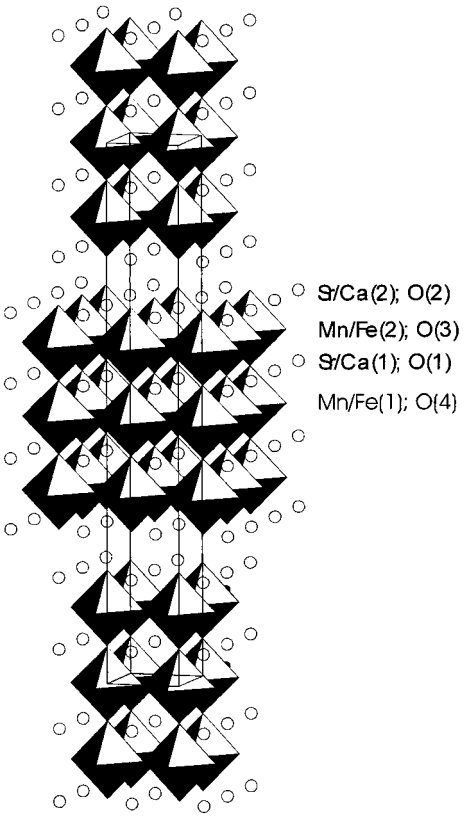

Figure 1. Schematic diagram of the $n = 3$ Ruddlesden−Popper structure of $Sr_{4-y}Ca_yMn_3O_{10-\delta}$ and $Sr_4Mn_{3-x}Fe_xO_{10-\delta}$.

$Ca_4Mn_3O_{10-\delta}$ phases.[13,14] We found that partial substitution of either Mn by Fe or Sr by Ca leads to a stable $n = 3$ RP phases (Figure 1) with $I4/mmm$ symmetry. These results prompted us to explore the phase limits of $Sr_4Mn_{3-x}Fe_xO_{10-\delta}$ and $Sr_{4-y}Ca_yMn_3O_{10-\delta}$ to achieve the stable $n = 3$ RP phase formation. The structure and properties of some of these compounds are also discussed in this paper.

Experimental Section

Synthesis. $Sr_4Mn_{3-x}Fe_xO_{10-\delta}$ was prepared by the solid-state reaction of $SrCO_3$ (99.9+%, Aldrich), Mn_2O_3 (Research ROC/RIC), and Fe_2O_3 (Fisher Scientific). Stoichiometric amounts of these starting materials were ground, pelletized, and fired in air at 1300 °C for 1 day, 1300 °C for another day, 1300 °C for 4 days, and then several times at 1400 °C for 5 days. The samples obtained after each firing were monitored by X-ray powder diffraction, and the heating was continued until the PXD patterns of the final phases were similar to those observed in the prior firing. The samples were reground and repelletized between each firing.

$Sr_{4-y}Ca_yMn_3O_{10-\delta}$ was synthesized both by solid state and sol−gel techniques, respectively. In the solid-state synthesis, stoichiometric quantities of $SrCO_3$ (99.9+%, Aldrich), $CaCO_3$ (99+%, Aldrich), and Mn_2O_3 (Research ROC/RIC) were mixed and ground. The reaction mixture was pressed into pellets and heated in air at 800 °C for 1 day, 1000 °C for 1 day, and 1300 °C for 7 days with two intermediate regrinding and repelletizing.

In the sol−gel synthesis, samples of $Sr_{4-y}Ca_yMn_3O_{10-\delta}$ were prepared from $SrCO_3$ (99.9+%, Aldrich), $CaCO_3$ (Aldrich, 99+%), and $Mn(NO_3)_2$ (0.9415 M solution, made from Mn metal and standardized). Stoichiometric amounts of the starting materials were dissolved in approximately 25 mL of 2 M HNO_3 to which an excess of citric acid (Aldrich, 99.5%) and ethylene glycol (Aldrich, 99+%) with respect to metal complex formation was added. After all the reactants were dissolved, the solution was heated on a hot plate, resulting in the formation of a gel. The gel was dried at 300 °C, then heated to 600 °C to remove the organic matter and to decompose the nitrates. The resultant ash was pressed into pellets and fired at 1300 °C for 8 days with three intermittent grindings and repelletizations. The final samples were quenched to room temperature.

Powder X-ray diffraction (PXD) data were collected with a SCINTAG PAD V diffractometer with monochromatized Cu Kα radiation over the range $4° \leq 2\theta \leq 110°$, with a step size of 0.02°. Rietveld refinement of the data was performed using GSAS.[15]

Electron Microscopy. The $Sr_{0.8}Ca_{3.2}Mn_3O_{10}$, $Sr_{1.15}Ca_{2.85}Mn_3O_{9.40}$, and $Sr_4Mn_{2.6}Fe_{0.4}O_{9.43}$ specimens were prepared for transmission electron microscopy (TEM) from sintered pellets by conventional polishing, dimpling, and ion thinning. The specimens were examined using a Phillips 430 (The use of brand or trade names does not imply endorsement of the product by the NIST.) electron microscope at 200 kV. High-resolution imaging was performed only for the $Sr_{1.15}Ca_{2.85}Mn_3O_{9.40}$ composition with a JEM3010 TEM microscope operated at 300 kV.

Magnetic susceptibilities of the samples were measured on a Quantum Design SQUID magnetometer over the temperature range 5−400 K in an applied magnetic field of 100 G. Data were collected by cooling in zero field (ZFC) and in an applied field (FC).

Resistivity measurements were made using a standard four-probe method over a temperature range of 50−350 K. Gold wire contacts were attached to the sintered polycrystalline samples with silver paint. The estimated uncertainty in the room-temperature resistivity (ρ_{RT}) is ∼20%.

The average oxidation state of manganese and iron was determined by iodometric titration.[16] The sample was dissolved in HCl, and excess KI was added prior to the dissolution and was oxidized by the sample to I_2. The formed I_2 was back-titrated with a standardized $Na_2S_2O_3$ solution. The entire iodometric titration process has to be carried out under an inert atmosphere (Ar/N_2) to avoid the formation of I_2 by oxidation in air. All the solutions were freshly made with distilled water that was boiled and subsequently cooled before use. Two or more parallel titrations were carried out to achieve good statistics.

Results and Discussion

The Synthesis and Analysis. Synthesis of $Sr_4Mn_{3-x}Fe_xO_{10-\delta}$ requires long heating times. The smaller the value of x, the longer the heating time needed to obtain a single RP phase. $Sr_4Mn_{3-x}Fe_xO_{10-\delta}$ with $x = 0.65, 0.70, 0.75$ are pure RP phases after the first firing at 1400 °C for 5 days; $Sr_4Mn_{3-x}Fe_xO_{10-\delta}$ with $x = 0.40, 0.45, 0.50, 0.60$ requires another firing at 1400 °C for 5 days for the formation of a single RP phase, while $Sr_4Mn_{3-x}Fe_xO_{10-\delta}$, $x = 0.10, 0.25, 0.30, 0.35$, do not convert to the RP structure even under repeated firing at 1400 °C. Thus, we conclude that under the conditions of our syntheses, the minimum Fe needed to stabilize the RP phase is $x \sim 0.40$. Figure 2a, a portion of which at 2θ between 41° and 50° is enlarged in Figure 2b, shows

(13) Fawcett, I. D.; Sunstrom, J. E., IV; Greenblatt, M.; Croft, M.; Ramanujachary, K. V. *Chem. Mater.* **1998**, *10*, 3643.

(14) Fawcett, I. D.; Veith, G. M.; Greenblatt, M.; Croft, M.; Nowik, I. *J. Solid State Chem.* **2000**, *155*, 96.

(15) Larson, A. C.; von Dreele, R. B. GSAS−Generalized Crystal Structure Analysis System, Los Alamos National Laboratory Report No. LA-UR-86-748, 1987.

(16) Licci, F.; Turilli G.; Ferro, P. *J. Magn. Magn. Mater.* **1996**, *164*, L268.

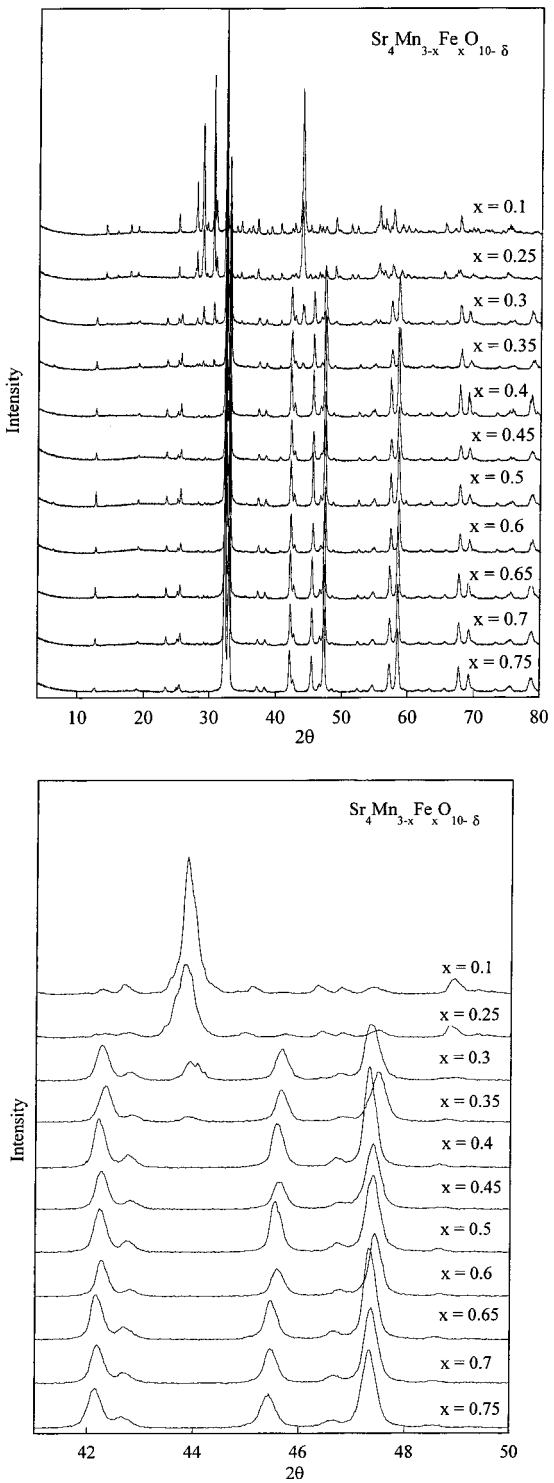

Figure 2. (a) Powder X-ray diffraction patterns of $Sr_4Mn_{3-x}Fe_xO_{10-\delta}$, $0.75 \leq x \leq 1.0$; (b) expanded 2θ PXD pattern of $Sr_4Mn_{3-x}Fe_xO_{10-\delta}$, $0.75 \leq x \leq 1.0$, in the range $40° \leq 2\theta \leq 50°$.

clearly the emergence of an unindexed peak at $\sim 44°$ for samples $Sr_4Mn_{3-x}Fe_xO_{10-\delta}$, $x \leq 0.35$.

$Sr_{4-y}Ca_yMn_3O_{10-\delta}$, $y = 1$, 1.5, 1.75, and 2, form mixtures of $n = 2$, 3, and ∞ RP phases. For example, in Figure 3, nominal "$Sr_3CaMn_3O_{10-\delta}$" is a mixture of $n = 2$, 3, and ∞ RP phases. The peak at $2\theta = 9°$ is a signature of the $n = 2$ RP phase.

$Sr_{4-y}Ca_yMn_3O_{10-\delta}$ was prepared by the sol−gel method as a RP single phase for $y \geq 2.85$. Figure 4a, a portion of which for 2θ between 5° and 20° is enlarged in Figure

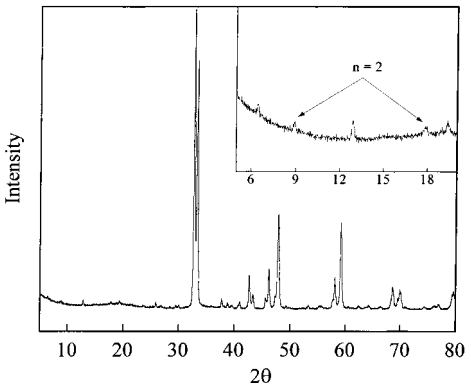

Figure 3. Powder X-ray diffraction patterns of nominal composition "$Sr_3CaMn_3O_{10-\delta}$" showing the presence of $n = 2$, 3, and ∞ phases.

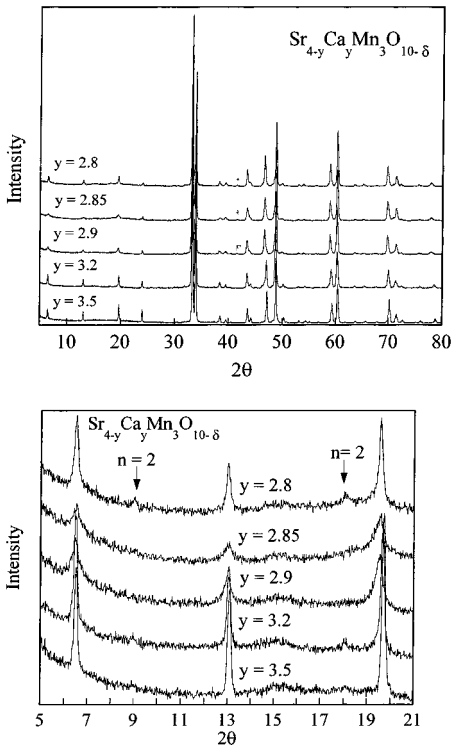

Figure 4. (a) Powder X-ray diffraction pattern of $Sr_{4-y}Ca_yMn_3O_{10-\delta}$ for $2.8 \leq y \leq 3.5$ showing the formation of $n = 3$ RP single phase for $y \geq 2.85$; (b) expanded 2θ PXD pattern $Sr_{4-y}Ca_yMn_3O_{10-\delta}$ for $2.8 \leq y \leq 3.5$ clearly showing the disappearance of the $n = 2$ RP for $y \geq 2.85$.

4b, shows the emergence of $n = 2$ RP phase peaks at $2\theta = 9°$ and 18° for $Sr_{1.2}Ca_{2.8}Mn_3O_{10-\delta}$. Thus, the minimum Ca needed to stabilize $Sr_{4-y}Ca_yMn_3O_{10-\delta}$ as a $n = 3$ RP phase is $y = 2.85$ by the sol−gel method. For samples prepared by solid-state methods, all the Sr must be replaced by Ca to obtain pure $n = 3$ RP phase ($y = 4$). For example, $Sr_{0.1}Ca_{3.9}Mn_3O_{10-\delta}$, i.e., $y = 3.9$, cannot be prepared as pure $n = 3$ RP phase by solid-state reaction; there are $n = 2$ and ∞ phases present.

The structural phase transition from $Sr_4Mn_3O_{10}$-type to RP-type at the critical Ca/Sr and Mn/Fe compositions respectively may be accounted for by considerations of the tolerance factor.

In $Sr_{4-y}Ca_yMn_3O_{10-\delta}$, for $y = 0$, the larger Sr^{2+} ion dictates face sharing of octahedra. In contrast, for $y = 2.85$ the tolerance factor favors corner-sharing octahedra stabilizing the RP structure. Similarly, the average

Table 1. Structural Parameters of $Sr_4Mn_{2.6}Fe_{0.4}O_{10-\delta}$ at Room Temperature[a]

atom	site	x	y	z	U_{iso} (Å^2)
Sr(1)	4e	0	0	0.5690(1)	0.0032(9)
Sr(2)	4e	0	0	0.7039(1)	0.031(2)
Mn/Fe(1)	2a	0	0	0	0.01[b]
Mn/Fe(2)	4e	0	0	0.1443(2)	0.01[b]
O(1)	4e	0	0	0.0626(6)	0.01[b]
O(2)	4e	0	0.5	0.2234(6)	0.01[b]
O(3)	8g	0	0.5	0.620(1)	0.49(2)
O(4)	4c	0	0.5	0.5	0.01[b]

[a] Space group $I4/mmm$; $a = 3.8409(1)$ Å, $c = 27.858(1)$ Å, $V = 410.98(4)$ Å^3. $R_{wp} = 14.19\%$, $R_p = 10.08\%$, $\chi_{red}^2 = 12.05$ for 33 variables. [b] U_{iso} was fixed during the refinement.

oxidation state of transition metal ions in the compound $Sr_4Mn_{2.6}Fe_{0.4}O_{9.43}$ is 3.62. If we assume that the valence of all of the Fe ions is 3+, then that of the Mn is 3.72+. Apparently this ratio of Mn^{3+}/Mn^{4+} in the perovskite layers is the appropriate effective radius to stabilize the RP phase over the $Sr_4Mn_3O_{10}$-type structure based on simple packing considerations of the tolerance factor.

The oxygen stoichiometries of several selected samples were determined by iodometric titration and result in the following formulations: $Sr_4Mn_{2.25}Fe_{0.75}O_{9.43}$, $Sr_4Mn_{2.6}Fe_{0.4}O_{9.43}$, $Ca_4Mn_3O_{9.43}$, and $Sr_{1.15}Ca_{2.85}Mn_3O_{9.40}$, with an error of ±0.04.

X-ray Structure Refinement. Rietveld refinements were carried out in tetragonal space group $I4/mmm$ with the parameters of $Sr_4MnFe_2O_{10-\delta}$[14] as an initial model. The background was modeled by Chebyschev polynomials of the first kind and the peak shape was described by a pseudo-Voigt function. Mn and Fe occupy the same sites, and their z parameters and isotropic thermal parameters were constrained to refine together. There are four oxygen sites in the $n = 3$ RP structure, and all four sites were assumed to have unit occupancy during the refinement. The positions with oxygen vacancies could not be located by PXD alone. For $Sr_4MnFe_2O_{10-\delta}$[14] neutron diffraction studies show that the oxygen vacancies are found mainly on the O1 [4e; 0 0 z] and O4 sites [4c; 0, 0.5, 0.5]; while Fe is located primarily on the 2a site [0 0 0]. During the refinement the occupancy factors of Mn/Fe on the two sites were fixed according to their stoichiometries, because of their indistinguishable electron scattering factors by X-ray. The results of the refinement for $Sr_4Mn_{2.6}Fe_{0.4}O_{9.43}$ are listed in Table 1 and the PXD patterns, including the raw data, the fitted profile, and the difference profile are shown in Figure 5a. $Sr_4Mn_{2.6}Fe_{0.4}O_{9.43}$ is monophasic at the resolution of a laboratory X-ray diffractometer, as no unidentified impurity peaks are observed.

The PXD data of $Sr_{1.15}Ca_{2.85}Mn_3O_{9.40}$ gave a better fit with the tetragonal space group $I4/mmm$ than with $Pbca$. It was shown that $Ca_4Mn_3O_{9.43}$ forms with space group $Pbca$, which is an orthorhombic distortion of the ideal $n = 3$ RP structure.[13,17] For the larger Sr^{2+} ions the Mn−O−Mn bond angles are close to the ideal 180° required for the $I4/mmm$ structure. Some ordering of Ca/Sr is also evident: the occupancy factors of Ca/Sr show that there is a larger fraction of the smaller Ca^{2+} ions in the Ca/Sr(2) 9-coordinated site and a larger fraction of the larger Sr^{2+} ions in the Ca/Sr(1) 12-coordinated perovskite site (Table 2, Figure 1). The refined structural parameters are listed in Table 2, and the observed and calculated diffraction patterns are plotted in Figure 5b. The relatively large χ^2 is mainly due to a much stronger higher angle of the doublet around 33° 2θ. This peak of the doublet overlaps with one of the $n = \infty$ perovskite peaks, suggesting that there may be up to 5% perovskite impurities in the sample. The electron microscopy investigations described below were undertaken to examine more accurately the phase purity of the samples.

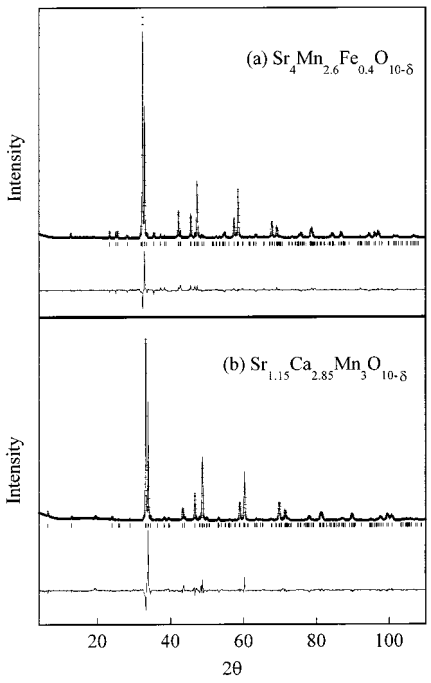

Figure 5. Typical X-ray diffraction profiles for (a) $Sr_4Mn_{2.6}Fe_{0.4}O_{9.43}$ and (b) $Sr_{1.15}Ca_{2.85}Mn_3O_{9.40}$. Key: observed data (+) and calculated profile (solid line); difference plots drawn below each profile, and tick marks represent allowed reflections.

Table 2. Structural Parameters of $Sr_{1.15}Ca_{2.85}Mn_3O_{10-\delta}$ at Room Temperature

atom	site	occupancy	x	y	z	U_{iso} (Å^2)
Ca/Sr(1)	4e	0.696(7)/0.304(7)	0	0	0.5663(2)	0.010(2)
Ca/Sr(2)	4e	0.729(7)/0.271(7)	0	0	0.7135(1)	−0.017(1)
Mn(1)	2a	1	0	0	0	0.023(3)
Mn(2)	4e	1	0	0	0.1497(2)	0.001(2)
O(1)	4e	1	0	0	0.0696(4)	−0.042(2)
O(2)	4e	1	0	0.5	0.2120(5)	0.025[b]
O(3)	8g	1	0	0.5	0.6305(5)	0.025[b]
O(4)	4c	1	0	0.5	0.5	0.20(2)

[a] Space group $I4/mmm$; $a = 3.7365(2)$ Å, $c = 27.230(2)$ Å, $V = 380.18(5)$ Å^3. $R_{wp} = 20.01\%$, $R_p = 14.17\%$, $\chi_{red}^2 = 16.35$ for 36 variables. [b] U_{iso} was fixed during the refinement, to avoid negative thermal parameters.

Electron Microscopy. For an ideal $I4/mmm$-type RP phase, the thickness of the perovskite blocks, i.e., the "n"-number, can be determined from selected area electron diffraction (SAD) patterns by counting the number of (00l) spots between a zero spot and a strong fundamental reflection corresponding to $(002)_p$ of cubic perovskite. The number of spots is equal to $2n$; therefore, for the $n = 3$ structure it is 6. Such six spots were seen consistently for all three studied compositions, which indicate that the dominant structure is the RP phase with $n = 3$. However, the sharpness of the (00l)

(17) Battle, P. D.; Green, M. A.; Lago, J.; Millburn, J. E.; Rosseinsky M. J.; Vente, J. F. *Chem. Mater.* **1998**, *10*, 658.

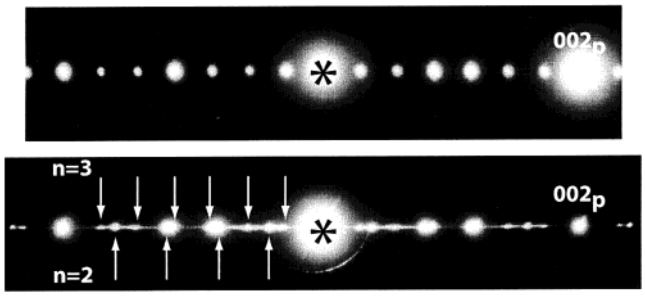

Figure 6. Selected area diffraction (SAD) patterns obtained from different grains of the $Sr_{0.8}Ca_{3.2}Mn_3O_{10-\delta}$ specimen. Arrows in b show the position of (00*l*) reflections for the RP $n = 2$ and 3 structures. According to the diffraction, grain a has well-ordered $n = 3$ structure, while grain b is a mixture of $n = 3$ and 2.

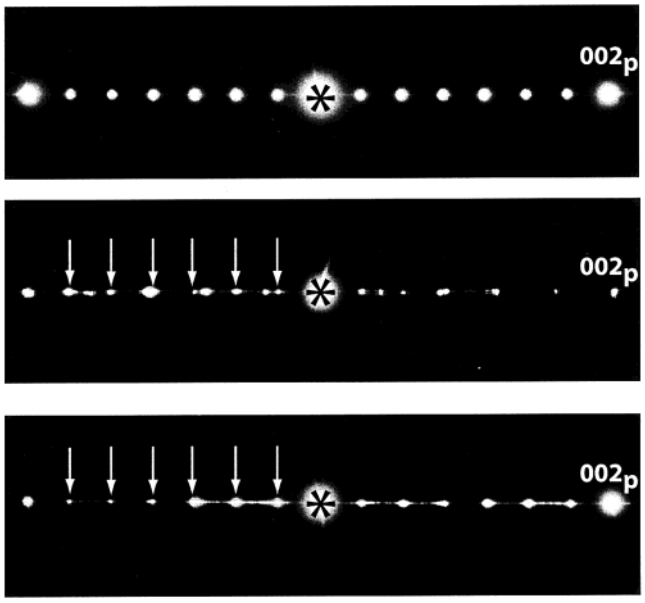

Figure 7. SAD patterns obtained from different grains of the $Sr_4Mn_{2.6}Fe_{0.4}O_{9.43}$ specimen. Similar to Figure 1, a is from a perfect $n = 3$ grain, b is a mixture of $n = 3$ and 2, while c is $n = 3$ with planar defects.

spots varies from grain to grain, which suggests a significant variation in the degree of stacking order.

Figure 6 shows typical examples of SAD patterns observed for different grains of the $Sr_{0.8}Ca_{3.2}Mn_3O_{10-\delta}$ sample. Spots on a SAD pattern in Figure 6a correspond to the well-ordered $n = 3$ structure. The SAD pattern in Figure 6b shows a distribution of spots that can be interpreted as a mixture of $n = 3$ and 2 (arrows in the figure indicate the ideal position of (00*l*) reflections for the RP $n = 2$ and 3 structures). Smearing of intensity in the *c**-direction suggests that the structures appear in a form of randomly mixed thin plates (with interface normal to *c**). SAD patterns for the $Sr_4Mn_{2.6}Fe_{0.4}O_{9.43}$ specimen (Figure 7) show a very similar picture: (a) a grain with the perfect $n = 3$ structure, (b) amixture of $n = 2$ and 3, and (c) $n = 3$ with intergrowth faults. Occasionally, intergrowth of the perovskite ($n = \infty$) layers with the $n = 3$ structure was also observed. Figure 8a shows a dark field image of a grain of $Sr_{1.15}Ca_{2.85}Mn_3O_{9.40}$ in which out-of-contrast lamellae are seen. The corresponding SAD pattern (Figure 8b) and the microdiffractions taken from a matrix (region A in part a) and from a lamella (B in part a) demonstrate that the lamellae have the perovskite structure (very large *n*). The observation of $^1/_2(110)$ reflections for the lamellae suggests an orthorhombic rather than cubic structure for the perovskite phase.

For a closer look into the intergrowth structure, we obtained high-resolution TEM images (HRTEM) for the $Sr_{1.15}Ca_{2.85}Mn_3O_{9.40}$ specimen. Figure 9 shows an example of such an image taken from a grain of $[010]_t$ orientation. Using phase-contrast simulation for the tetragonal RP structures and fast Fourier transform (FFT) from selected regions of the HRTEM image, the structure was analyzed as consisting of predominately $n = 3$ regions (e.g., region A and the corresponding FFT). In addition, individual perovskite blocks with $n = 2$, 5, and 7 were identified (see labeling of the blocks around the periphery of the image). According to the imaging, all perovskite-type blocks are connected with each other through a rock salt layer.

In addition to the reflections of a tetragonal RP phase, for the $Sr_{1.15}Ca_{2.85}Mn_3O_{9.40}$ composition, the ($^h/_2$ $^k/_2$ *l*) rows of a continuous intensity were observed (Figure 10). Note that in this SAD pattern the reflections of the tetragonal *I*4/*mmm* lattice are sharp, with the exception of intensity streaks due to partial intergrowth. The presence of reflections in addition to those corresponding to the tetragonal structure suggests an orthorhombic superstructure, which apparently forms during cooling of the specimen from the high sintering temperature. A similar superstructure was observed for the recently studied $La_{2-2x}Ca_{1+2x}Mn_2O_7$ manganates in the composition range $0.8 < x < 1.0$.[18] For $La_{2-2x}Ca_{1+2x}Mn_2O_7$ a structural model based on tilting of octahedra was suggested. Work is in progress to establish a more detailed picture of the origin and nature of the observed superstructure.

TEM results usually suffer from poor statistics, because of the observation of a limited number of individual grains, and it can be significant for inhomogeneous materials. In our case we observed about 10 grains per each composition. We conclude that about 50% of the grains have the well-ordered $n = 3$ structure. The rest of the grains show significant intergrowth between the $n = 2$ and 3 structures, with predominantly blocks of $n = 3$ layers. Only occasionally the formation of perovskite ($n = \infty$) blocks was observed.

Magnetic Results. $Sr_4Mn_{3-x}Fe_xO_{10-\delta}$ ($0.4 \leq x \leq 3$) is semiconducting and antiferromagnetic. A typical temperature dependence of the magnetic susceptibility [χ(T)] of $Sr_4Mn_{2.6}Fe_{0.4}O_{9.43}$ is shown in Figure 11a. There is divergence in the FC and ZFC susceptibilities at low temperature, typical of the spin-glass-type behavior seen in other $n = 3$ RP phases.[14,19] The high-temperature susceptibility (150−400K) data was fitted to the Curie−Weiss law [($\chi = C/(T - \theta)$], with the constants $C = 9.59$ emu K/mol and $\theta = -221$ K; the large negative θ suggests antiferromagnetic (AF) behavior.

(18) Seshadri, R.; Hervieu, M.; Martin, C.; Maignan, A.; Dominges, B.; Raveau, B.; Fitch, A. N. *Chem Mater*. **1997**, *9*, 1778.
(19) Sloan, J.; Battle, P. D.; Green, M. A.; Rosseinsky, M. J.; Vente, J. F. *J. Solid State Chem*. **1998**, *138*, 135.
(20) Laffez, P.; Van Tendeloo, G.; Seshadri, R.; Hervieu, M.; Martin, C.; Maignan, A.; Raveau, B. *J. Appl. Phys*. **1996**, *80*, 5850.
(21) Bendersky, L. A.; Chen, R.; Fawcett, I. D.; Greenblatt, M. J. *Sol. State Chem. M*. **2001**, *157*, 309.
(22) Battle, P. D.; Brandford, W. R.; Mihut, A.; Rosseinsky, M. J.; Singleton, J.; Sloan, J.; Spring, L. E.; Vente, J. F. *Chem. Mater*. **1999**, *11*, 674.

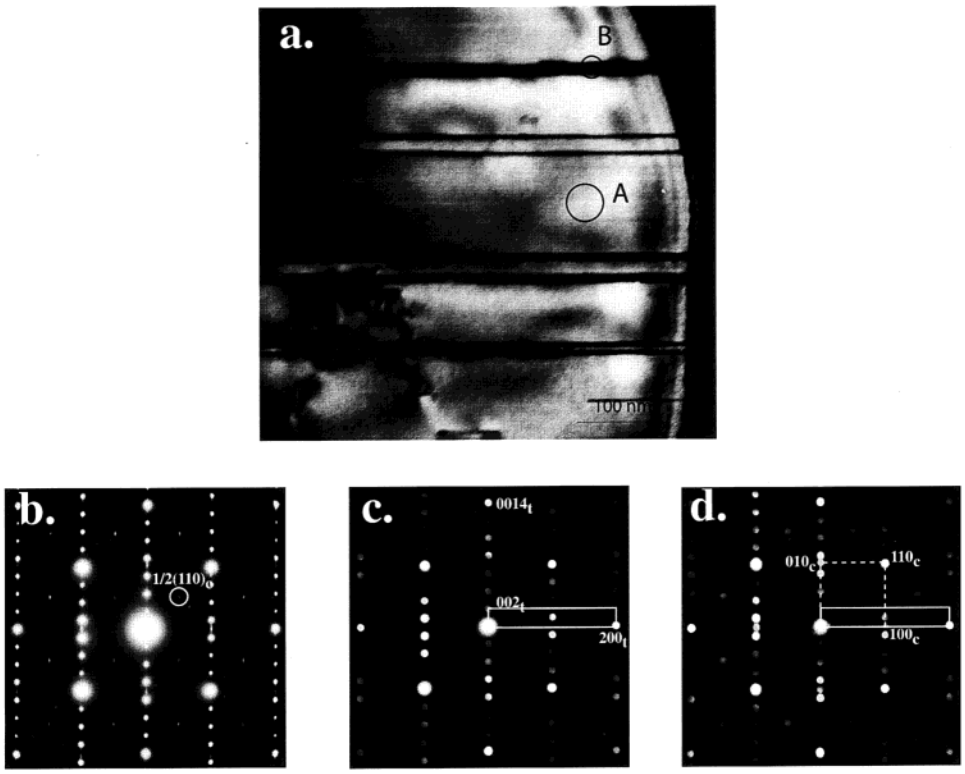

Figure 8. (a) A dark field image of a grain of $Sr_{1.15}Ca_{2.85}Mn_3O_{9.40}$ with out-of-contrast lamellae. (b) The corresponding $[010]_t$ SAD pattern. (c, d) Microdiffractions taken from regions A and B, respectively corresponding to $n = 3$ and perovskite. Observation of the $^1/_2(110)$ reflections in b suggest orthorhombic distortions of the perovskite phase.

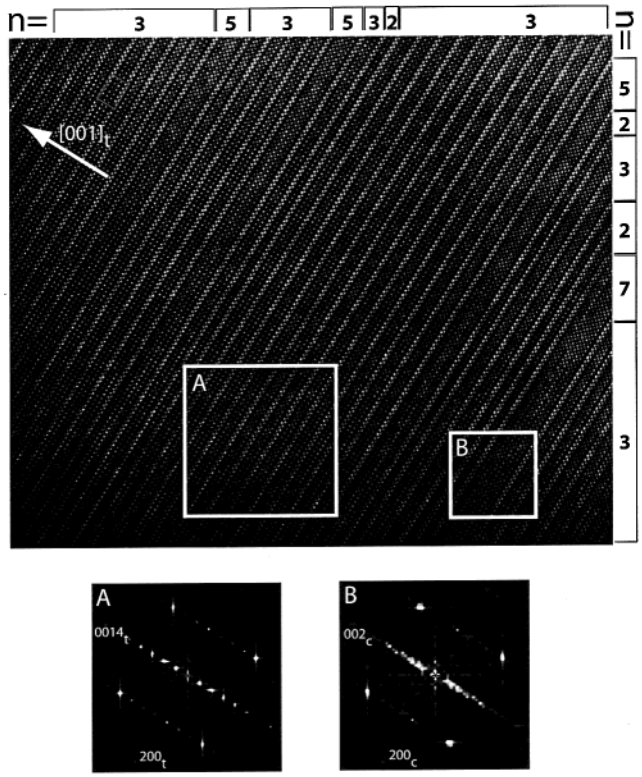

Figure 9. High-resolution TEM image obtained for the $Sr_{1.15}Ca_{2.85}Mn_3O_{9.40}$ specimen at $[010]_t$ orientation. Individual perovskite blocks were identified and labeled around periphery of the image. Fast Fourier transforms from selected regions A and B of the image are shown at the bottom.

$Sr_{4-y}Ca_yMn_3O_{10-\delta}$ ($2.85 \leq y \leq 4$) also exhibits semiconducting and antiferromagnetic behavior. A typical temperature dependence of the magnetic susceptibility

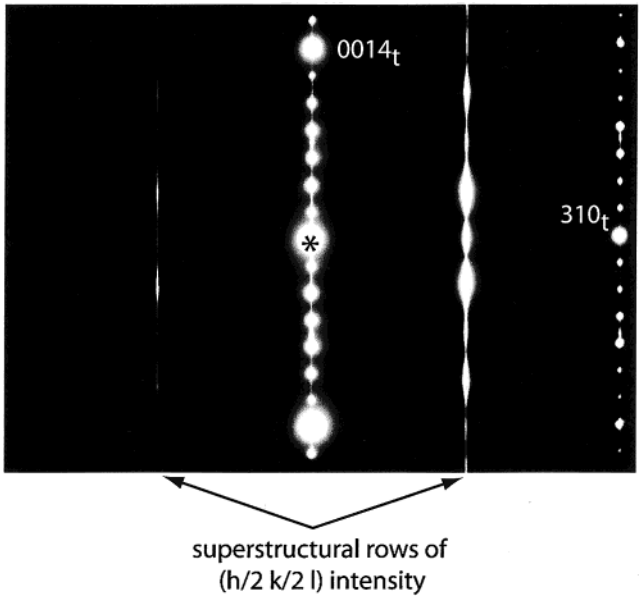

Figure 10. $[310]_t$ SAD pattern obtained from $Sr_{1.15}Ca_{2.85}Mn_3O_{9.40}$. In addition to the reflections corresponding to the tetragonal RP $n = 3$ phase, ($^h/_2$ $^k/_2$ l) rows of intensity are also observed. Note that the reflections of the tetragonal $I4/mmm$ lattice are sharp in comparison to near continuous extra rows.

[χ(T)] as $Sr_{1.15}Ca_{2.85}Mn_3O_{9.40}$ is shown in Figure 11b. Again, divergence in the FC and ZFC susceptibilities is observed at low temperatures, which suggests the spin-glass-type behavior seen in other $n = 3$ RP phases.[14,19] The high-temperature susceptibility (150−400 K) data were fitted to the Curie−Weiss law, with constants $C = 8.56$ emu K/mol and $\theta = -811$ K; the very large value of θ is too large to be due to AF intereactions alone and is indicative of covalent effects.

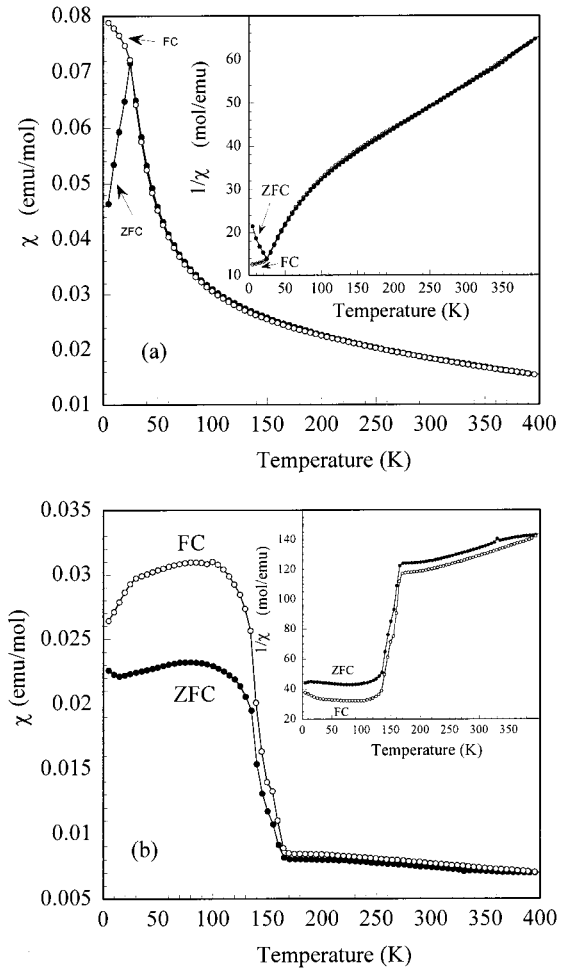

Figure 11. The temperature dependence of the magnetic susceptibility for (a) $Sr_4Mn_{2.6}Fe_{0.4}O_{9.43}$ and (b) $Sr_{1.15}Ca_{2.85}Mn_3O_{9.40}$. Inset: inverse susceptibility vs temperature.

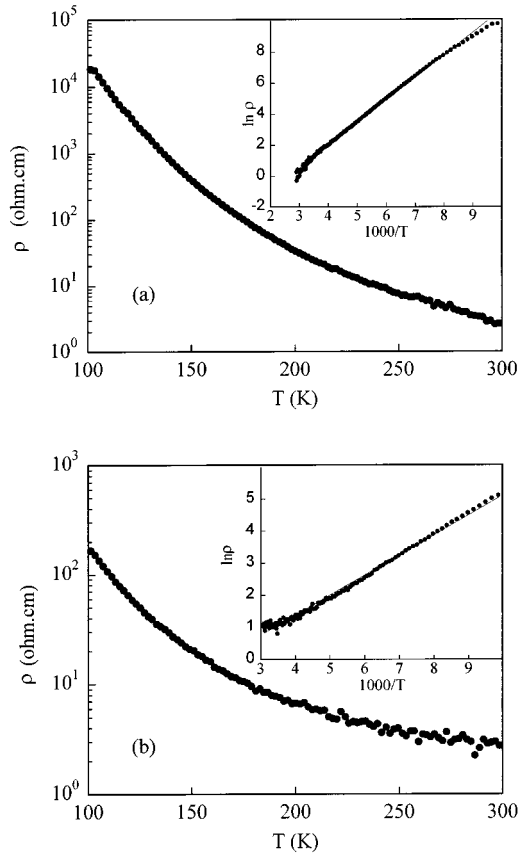

Figure 12. The temperature dependence of the resistivity, ln(ρ) vs T for (a) $Sr_4Mn_{2.6}Fe_{0.4}O_{9.43}$ and (b) $Sr_{1.15}Ca_{2.85}Mn_3O_{9.40}$. Inset: ln($\rho$) vs 1000/$T$.

The temperature dependence of the resistivity, ln(ρ) vs 1/T, for $Sr_4Mn_{2.6}Fe_{0.4}O_{9.43}$ shown in Figure 12a indicates semiconducting behavior in the temperature range measured with $\rho_{RT} \sim 3\ \Omega$ cm. The activation energy for conduction (E_a) was determined to be 0.125 eV from the slope of the ln(ρ) vs 1/T in the temperature range 100−300 K. Similarly, Figure 12b shows that $Sr_{1.15}Ca_{2.85}Mn_3O_{9.40}$ is a better semiconductor at room temperature ($\rho_{RT} \sim 2\ \Omega$ cm) with $E_a = 0.054$ eV.

Conclusion

The minimum amount of Fe required to obtain a stable Ruddlesden−Popper phase for $Sr_4Mn_{3-x}Fe_xO_{10-\delta}$ is $x = 0.40$, and the minimum amount of Ca needed to stabilize the RP structure for $Sr_{4-y}Ca_yMn_3O_{10-\delta}$ is $y = 2.85$. Both phases are semiconducting, with strong antiferromagnetic interactions and spin-glass-type behavior at low temperature. TEM studies evidence that about 50% of the grains have well-ordered $n = 3$ structure for both series of RP phases investigated. The rest of the grains show significant intergrowth between $n = 2$ and 3 structures, with predominantly blocks of $n = 3$ layers, and only occasionally the formation of perovskite ($n = \infty$) blocks was observed.

Acknowledgment. This work was supported by National Science Foundation-Solid State Chemistry Grant DMR-99-07963. The authors thank Professor W. H. McCarroll for critical reading of the manuscript.

CM0102842